international journal of aeroacoustics volume 2 · number 1 · 2003 – pages 35 – 63

Effects of vortex generating tabs on noise sources in an ideally expanded mach 1.3 jet

J. Hileman and M. Samimy

Gas Dynamics and Turbulence Laboratory, Department of Mechanical Engineering, The Ohio State University, Columbus, Ohio 43210

samimy.1@osu.edu

ABSTRACT

The flow and acoustic fields of an ideally expanded Mach 1.3 axisymmetric jet with delta tabs were examined to explore the effects of the tabs on noise sources. This work continues research that was performed on a baseline (no-tab) jet. Noise measurements were made at an angle of 30˚ to the downstream jet axis to allow a direct comparison to previous work, and to relate the sound generation mechanisms to the large structures that were visualized with temporally resolved flow visualization. Additional acoustic measurements were made at 60˚ and 90˚ locations. Three cases were examined: a baseline jet, a single delta tab jet, and a dual delta tab jet. Both tab jets were operated at the same pressure ratio as the baseline jet, which was ideally expanded. Power spectra and average acoustic waveform measurements were made for a variety of azimuthal locations; apparent noise origins were estimated with a 3-D microphone array; and temporally resolved flow visualization was used to examine the dynamic flow structure of the jet's mixing-layer. The results confirm that the tabs generate strong streamwise vortices that have a significant effect on both the flow and acoustic fields of the jet. The tabs cause significant deformation in the cross-stream plane of the mixing-layer, as well as regulating the formation and roll-up of vortices due to Kelvin Helmholtz instability. With the addition of tabs, the noise field becomes azimuthally dependent and the region of noise generation moves dramatically upstream. It appears that the tabs are directly responsible for an increase in noise over a range of Strouhal numbers between 0.8 and 2.5 through generated streamwise vortices and they are indirectly responsible for the modification of the noise generating mechanisms at Strouhal numbers below 0.6 through the induced spanwise vortex roll-ups.

ACRONYMS AND SYMBOLS

D	Jet diameter, equivalent to 1 inch (0.025 m)
σ	Standard deviation of acoustic pressure
St_D	Strouhal number based on jet diameter
SPL	Sound pressure level (given in dB)
U	Jet exit velocity, equivalent to 380 m/s
U_c	Convective velocity for the jet, equivalent to 270 m/s

1. INTRODUCTION

Since the start of commercial jet travel, aircraft noise has been a nuisance to those living near airports or under flight paths. The exhaust of jet engines is responsible for the majority of noise during the take-off phase of a jet aircraft, and as such has been a topic of research over the past fifty plus years. Significant gains have been made in reducing the noise from jet exhaust by following Lighthill's 8th power law [1], which shows the overall radiated acoustic power from a jet's exhaust is proportional to the eighth power of its exit velocity. By utilizing larger by-pass ratio engines, the effective velocity of the exhaust has been significantly reduced, and the noise levels have dropped. However, additional reductions in noise levels are required and the exhaust velocities of today's engines cannot be lowered much further. As such, different approaches are required for noise reduction. This work is a continuation of research that has focused on how large turbulence structures create noise [2-3]. It is expected that more effective noise control strategies could be developed with such knowledge. The specific focus of this work is how vortex-generating tabs modify the noise generation mechanisms of an ideally expanded, high-speed jet.

The noise from an ideally expanded jet has been traditionally thought to have two principal components. One component radiates preferentially in the downstream direction and is associated with the large-scale turbulence structures within the jet's mixing-layer. The other component comes from the small-scale turbulence structures and radiates uniformly in all directions. The exact nature of the mechanisms for the two components is not well understood, but their difference is apparent when sound spectra from various measurement angles are compared. For the baseline (no-tab), Mach 1.3 jet of this study, the sound radiation over a region that is normal to the jet axis is uniform over most frequencies; however, at shallow angles (around 30˚, as measured from the downstream jet centerline), the acoustic spectrum has a broadband peak between 2 and 4 kHz (St_D = 0.13 to 0.27) [2]. This low frequency, large amplitude peak has been associated with the large-scale structures of the flow. Since such structures are the easiest to measure and ultimately to manipulate, the current jet aeroacoustics work at the Gas Dynamics and Turbulence Laboratory has focused on sound measurements made at the 30˚ location. The main objective of this long-term study is to relate the sound generation to time-dependent processes of these structures.

In a baseline jet, the large amplitude turbulent mixing noise originates mostly from a region surrounding the end of the potential core [3-7]. The higher frequency noise appears to emanate from nearer the jet exit, while lower frequency noise comes from regions of the flow that are further downstream [8-10]. In studies of low-speed jets and mixing-layers, the noise creation process has been linked to vortex pairing [11-13]. However, Bridges and Hussain [14] argue that for vortex pairing to be the dominant noise generation mechanism in low-speed jets, the pairing needs to be asymmetric. A direct numerical simulation of a low Reynolds number, Mach 0.9 jet showed the far-field noise originates from a region where the computed Lighthill noise sources were both strong and rapidly changing in time [15]. Sarohia and Massier [16] performed experiments using high-speed schlieren motion pictures that were synchronized with

near-field pressure measurements. Their study of excited subsonic jets with Mach numbers ranging from 0.1 to 0.9 and Reynolds number up to 10^6 found that large instantaneous pressure pulses were formed whenever two large-scale structures merged; however, the passage of a large structure did not significantly change the near-field pressure signal. These results support the idea that an event with *significant* temporal variation is required to generate noise. By utilizing noise source localization with simultaneous far field acoustic measurements and temporally resolved flow visualizations on the baseline Mach 1.3 jet used in this study, Hileman et al. [2-3] inferred three noise generation mechanisms: large structure roll-up, significant interaction between structures on opposite sides of the jet mixing-layer, and large structure tearing. All of these mechanisms involve dynamic (time-varying) processes. The convective velocity for the baseline jet of this study was measured as 270 m/sec [17]; therefore, this jet should not be creating Mach wave radiation.

One effective means of significantly modifying the mixing and acoustic properties of a jet is to introduce strong, streamwise vortices to the flow via small tabs placed at the nozzle exit. Tabs were initially examined because of their ability to eliminate the screech tone from non-ideally expanded supersonic jets (e.g., references 18 and 19). The first research that analyzed how tabs affect the flow field of a round jet was conducted on a low subsonic jet [20] and this was followed by work on high subsonic and underexpanded supersonic jets [18]. Both of these studies used varying numbers of rectangular shaped tabs, and they both agreed that tabs caused: (1) the potential core of the jet to significantly shorten, (2) the loss of the jet's axisymmetric character, and (3) increased entrainment of ambient air. The flow visualizations of Samimy et al. [19] showed the dramatic effect of tabs on round jets. Their cross-stream flow images showed that with two tabs, the jet was bifurcated; and additional tabs caused the jet to develop a corresponding number of 'fingers' that completely distorted the jet. These drastic changes in the jet are known to be caused by the presence of strong, counter-rotating streamwise vortices. The presence and properties of these vortices were observed in flow visualizations [19], measured in a Mach 0.3 jet via hot-wire anemometry [21], measured in a low-speed jet via laser Doppler velocimetry [22], and were quantitatively shown to exist in Mach 1, 1.5, and 2 ideally expanded jets via filtered Rayleigh scattering measurements [23], as well as in an underexpanded supersonic jet via 3-D planar Doppler velocimetry measurements [24]. The most effective tabs have a triangular shape, are located at the nozzle exit, and are inclined at a 45˚ angle to the downstream axis [21]. The effectiveness of this configuration, which is referred to as a 'delta tab,' is due to the mechanisms that create the strong, streamwise vortices. The primary source of the streamwise vorticity is the pressure hill that develops upstream of each tab. A secondary source is the shedding of vortex filaments from the sides of the tab [21]. When the tabs are inclined in the downstream direction, these two sources augment each other. Two delta tabs are shown in the two schematics of Figure 1, and the direction of the induced streamwise vortices are shown relative to a delta tab in Figure 2.

Research has been conducted to determine the effect of delta tabs on the acoustic far-field of heated and unheated Mach 0.9 round jets [8, 25]. Based on their results,

there is not a significant change in the sound levels perpendicular to the jet nozzle exit caused by the addition of multiple tabs (up to 8), but there is a shift in the peak frequency. In the downstream direction, adding multiple tabs causes a decrease in the sound level of lower frequencies, but there is a corresponding increase in sound level at higher frequencies. Based on these results, it is apparent that tabs affect the sound generation of ideally expanded jets, but the question of *how* such tabs modify the noise generation mechanisms has not been answered.

The focus of this work is to examine how delta tabs are modifying the noise generation mechanism in a Mach 1.3, ideally expanded jet. Three cases are examined and compared: (1) a baseline (no-tab) jet, (2) a single delta tab jet, and (3) a dual delta tab jet, where the tabs are located on opposite sides of the jet. Both delta tab jets were operated at the same pressure ratio as the baseline jet, which was ideally expanded. The acoustic field was examined at downstream angles of 30, 60 and 90˚ with noise source estimation being performed with a 3-D microphone array. Flow images were taken of both cross-stream and streamwise planes. The rest of this paper is divided into the following: a brief account of the experimental setup, an examination of the average properties of the jets (both acoustic and flow field), temporally resolved flow visualizations, and finally conclusions.

2. EXPERIMENTAL ARRANGEMENT

2.1. Jet facility and anechoic chamber

The air for the Mach 1.3 jet was supplied by two four stage compressors; it was filtered, dried, and stored in two cylindrical tanks with a total capacity of 42.5 m^3 at a pressure of 16.5 MPa (1600 ft^3 at 2500 psi). A stagnation chamber was used to condition the jet air before exhausting it through a 25.4 mm (1 inch) nozzle with a lip thickness of 2.5 mm (0.1 in) where the inner contour was determined by the method of characteristics for uniform flow at the exit. The actual Mach number of the nozzle was measured as 1.28 and the Reynolds number for the jet based on the nozzle exit diameter was $1.08x10^6$. The delta tabs used in this experiment were designed to extend into the flow at an angle of approximately 45˚. A schematic of the tabs mounted at the exit of the nozzle is shown in Figure 1. As shown in the schematic, each tab extends 1/8 D into the stream, and is 1/4 D wide at the base. Based on these dimensions, each tab blocks about 2% of the exit area of the jet. This is a similar area blockage as that used in reference 21. A single small screw mounted the tabs; hence, the exact dimensions might have varied from the given specifications. The tabbed jets were operated at the same pressure ratio as the baseline jet.

All of the experiments were conducted within the optically accessed anechoic chamber of the Gas Dynamics and Turbulence Laboratory. The chamber was tested for compliance to ANSI Standard S12.3535, and the results from the tests were within the required tolerance over most of the distances along the microphone paths [26]. The inner dimensions of the chamber measure, from wedge tip to wedge tip, 3.12 meters in width and length, and 2.69 meters in height. Additional details of the anechoic chamber and jet flow facility can be found in references 2 and 26.

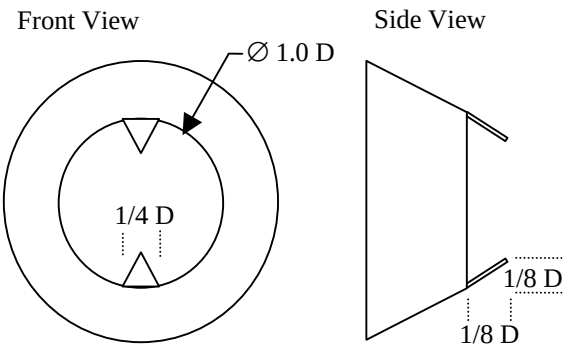

Figure 1. Schematic of two delta tabs mounted on a nozzle. The dimensions used are shown in jet diameters. Schematic is not to scale.

2.2. 3-D microphone array

The purpose of this line of research is to relate the *dynamics* of large turbulence structures to the emission of sound. Conventional methods of noise source localization that rely on analysis of the frequency domain will not work as they yield an average source location. What is needed is a temporal domain analysis where the origin of *individual* sound events can be determined. Based on this special need, a novel approach was taken in the design of an acoustic array. It works by measuring the phase lag of individual sound events between microphones in space. With this phase lag information and the geometry of the array, a sound origin is determined for every acoustic event that exceeds a set amplitude threshold.

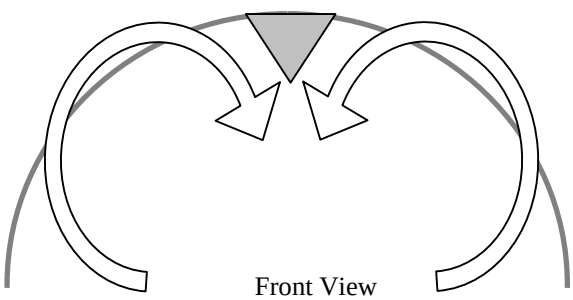

Figure 2. Direction of the streamwise vortices that are induced by a single delta tab. View is from downstream of the tab, and the upper half of the nozzle of Figure 1 is shown.

The present 3-D microphone array/analysis algorithm is a third-generation design that measures the time difference between spatially distributed microphones recording an individual acoustic peak. The first generation array consisted of two microphones aligned with the jet centerline, separated by 5 nozzle exit diameters (12.7 cm), and

placed at a 30˚ location. This array was used with dual pulse flow visualization in reference 2. The second-generation array expanded the number of microphones to four with a total aperture of 6 nozzle exit diameters (15.2 cm). It was used in conjunction with real-time flow visualization in reference 3. The third generation design consists of eight microphones (¼ inch B&K 4135 and 4939 microphones) placed in three-dimensional space as shown in the schematic of Figure 3. Six of the microphones (microphones 1, 2, 4-6, 8 of Figure 3) were equally spaced around the periphery of the ring to determine the far field noise origin in the cross-stream plane, while two sets of microphones (microphones 2&3, 6&7) were aligned with the jet centerline to determine the streamwise origin. A plasma arc was used to test the 3-D microphone array's ability to locate noise sources of varying frequency content. The arc created an acoustic tone that could be precisely controlled between a few hundred Hertz and 20 kHz. The 3-D microphone array was able to accurately locate the plasma arc when it was producing acoustic frequencies under 10 kHz. The array was then evaluated using a fluidic device that was creating a narrowband (3 kHz tone) as well as broadband (between 1 and 10 kHz) acoustic radiation. Based on the array's inability to locate noise sources having frequencies above 10 kHz, the acoustic data was low pass filtered at this frequency using a fifth order Chebyshev type I digital filter. Further details of the array, the associated noise source location algorithm, and its calibration can be found in reference 27.

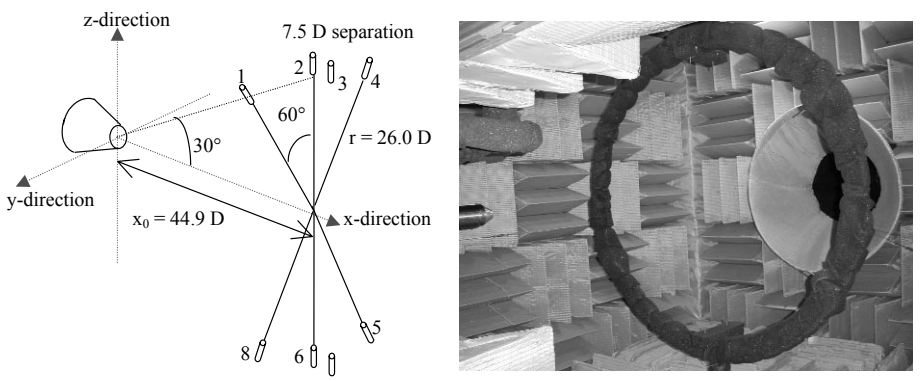

Figure 3. Schematic and photograph of the 3-D microphone array that is used to locate noise sources in space.

2.3. Temporally resolved flow visualization

The flow was visualized via scattering of laser light by condensed water particles within the mixing-layer of the jet. The warm, moist air of the ambient is entrained into the cold, dry jet air that is exiting the nozzle, thus forming the jet's mixing-layer. Upon mixing, the moisture contained in the ambient air condenses into small particles that mark the majority of the mixing-layer. An in-house, custom-built pulse burst laser was used to create a laser sheet, and the scattered light from the condensed particles was captured with a camera from Silicon Mountain Design (SMD, now a subsidiary of Dalsa Inc.). Both the laser and the camera are capable of operating at a MHz rate. The

camera was placed inside of the chamber, perpendicular to the laser sheet for the streamwise images, and it was placed at an angle of about 30˚ with respect to the jet axis to capture the cross-stream images. The flow visualization sets in this work consist of images that were separated by 8 μsec (125 kHz). Further details of this laser/camera system can be found in reference 17.

3. RESULTS

3.1. Average flow images

Average images of the tabbed jet will be compared with those of the baseline (no-tab) jet. Figure 4 shows two average images of the baseline jet. The downstream distance from the nozzle exit is given at the bottom of the images in terms of number of nozzle exit diameters. Image (a) shows the baseline Mach 1.3 jet over a range of downstream locations from 2.5 to 8 x/D while image (b) shows the same jet from 5.5 to 11 x/D. The bright regions are the two sides of the mixing-layer, and the dark region between them is the unmixed core of the jet. As mentioned in the last section, the visualization of the mixing regions is accomplished by scattering of light from a laser sheet by moisture particles within the mixing region. This technique visualizes a major portion of the mixing region, but it does not illuminate the entire mixing-layer. Therefore, the core of unmixed fluid is longer than the actual potential core of the jet as measured using a pitot probe, which was found to be about 5.5 x/D for the baseline jet [2]. Two average images of the single delta tab jet are shown in Figure 5 for a range of downstream locations from 1 to 5 x/D; the tab location is at the top of the nozzle in (a) and at the bottom of the nozzle in (b). The tab side of the mixing-layer has been deflected away from the tab, and the opposite mixing-layer is fairly unaffected until the two sides interact downstream of 3 x/D. This marks the end of the unmixed core region. Figure 6 shows two average images of the dual-tab jet over a similar range of downstream locations (1 to 5 x/D). The plane passing through the tabs is shown in (a), while the tab-normal plane is shown in (b). The tab-normal plane image shows that the mixing-layer is bifurcated with two unmixed cores that end around 3 x/D. The difference in the length of the unmixed core of the tabbed and tab-normal planes of Figure 6 is likely due to the difference in the relative intensities of the images.

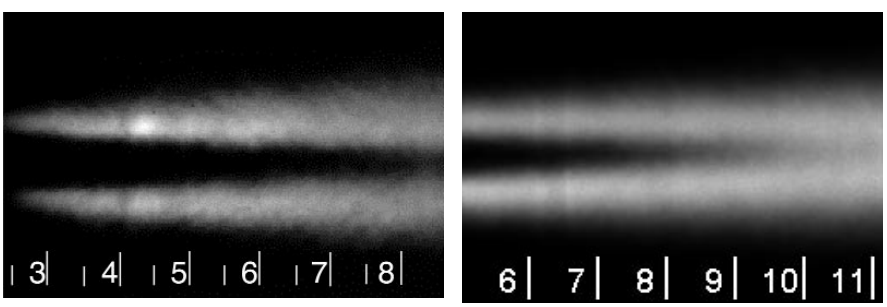

(a) (b)

Figure 4. Average streamwise image of the baseline (no-tab) jet. Downstream distances are marked along the top of the image in x/D.

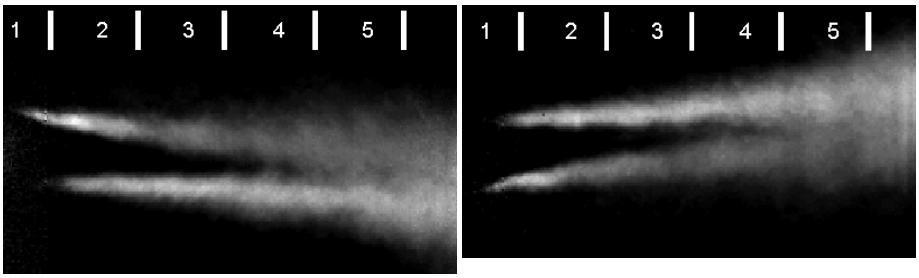

(a) (b)

Figure 5. Average streamwise images for a single-tab jet. The tab was on the top lip of the nozzle for (a) and at the bottom lip of the nozzle for (b).

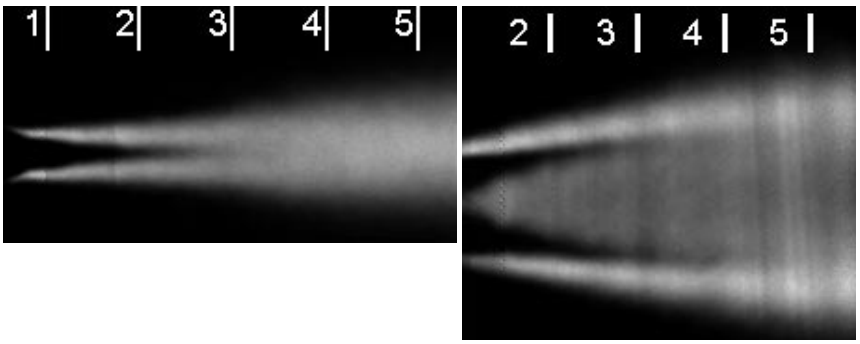

(a) (b)

Figure 6. Average streamwise images of a dual-tab jet. The illuminating and tab planes coincide in (a) and are normal in (b).

Cross-stream images of the jet were taken at a downstream location of 3 x/D. Image (a) of Figure 7 shows the average cross-section of the baseline jet. As would be expected, the mixing-layer is round with a relatively uniform thickness - the variation is due to small sample size. Image (b) of Figure 7 shows the average single-tab jet taken at the 3 x/D location. The delta tab, which is located at the top of the nozzle, has dramatically changed the cross-section of the jet and transformed it into a 'crescent' shape. The pair of strong streamwise vortices that were generated by the tab has contorted the top of the jet's mixing-layer while the bottom has remained relatively uniform. When a second delta tab is added to the nozzle, as is the case for image (c) of Figure 7, a second set of strong streamwise vortices is created, and the cross-section becomes pinched along the vertical axis (a line connecting the two tabs). This caused the bifurcation of the unmixed core that was observed in Figure 6.

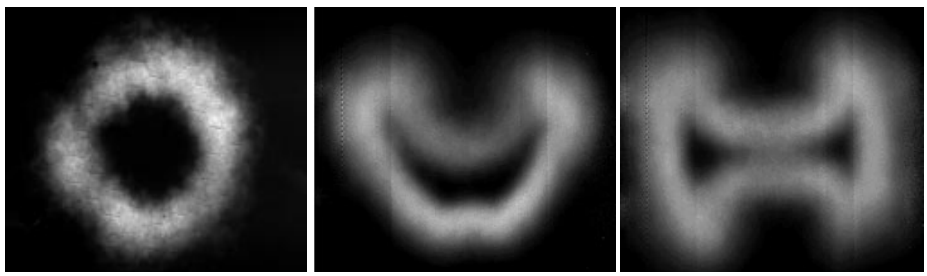

(a) No tab (b) Single-tab (c) Dual-tab

Figure 7. Average cross-stream images at a downstream distance of 3 x/D. Image (a) is for the baseline jet. Image (b) is a single-tab jet where the tab was located at the top lip of the nozzle. Image (c) is a dual-tab jet where the tabs were at the top and bottom lips of the nozzle.

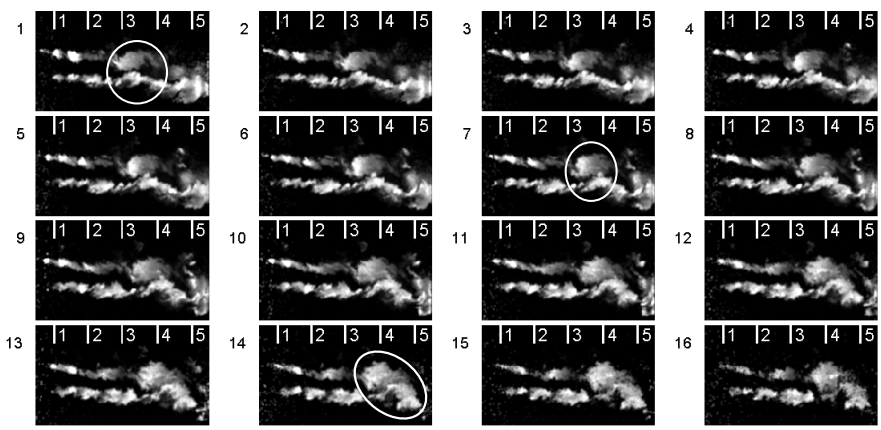

Figure 8. Example of a streamwise image set from a single-tab jet showing a structure roll-up that significantly interacts with the opposite side of the mixing-layer. The roll-up and area of interaction are within the circled regions of frames 1, 7 and 14. Tab is on the top lip of the jet nozzle.

3.2. Instantaneous flow images

Figure 8 shows 16 images that depict the streamwise development of the jet mixing-layer. The downstream distances are given next to the tic marks in terms of number of nozzle exit diameter, and the frame numbers are given next to the individual images. This region of the jet shows a typical structure roll-up for the single-tab jet. The roll-up is occurring in the upper half of the mixing-layer between 3 and 4 x/D over the course of the frames. The circle in frame 1 shows the roll-up and a region of the bottom mixing-layer that is being affected by the roll-up. This rolling-up structure induces an upward bend in the lower part of the mixing-layer. This process is well under way in the circled region of frame 7. As the structure becomes larger, it starts interacting with

the deformed section of the opposite side of the mixing-layer, where a roll-up of opposite sign, but not as strong is induced (this is shown in the circle of frame 14). These interacting rolling-up structures were a regular feature of the flow image sets.

Upstream of 3 x/D, the development of the dual-tab jet is dominated by staggered roll-ups that form on opposite sides of the mixing-layer. This aspect is captured in the instantaneous flow images of Figure 9. Two roll-ups are shown in the oval of frame 7. Figure 10 shows two instantaneous, streamwise images of the dual-tab jet over a larger downstream range. Image (a) shows the tab-plane (similar to the ones shown in Figure 9), while image (b) is of a plane normal to the tabs. The two images were not taken simultaneously. The roll-ups that were the focus of Figure 9 are also present in image (a) from Figure 10 and are within the central region of image (b) from Figure 10. Downstream of 3 x/D, the dual-tab jet is dominated by larger structures that span a significant part of the height and width of the jet. This region is quite dynamic with strong three-dimensionality. The two images of Figure 10 show a wide variety of large turbulence structures and structure interactions that are present in this dynamic region.

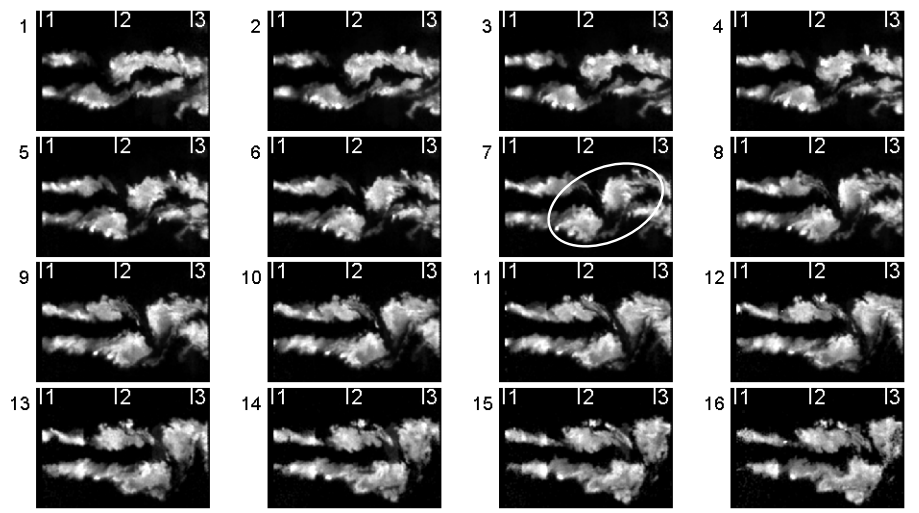

Figure 9. Example of a streamwise image set from a dual-tab jet showing a structure roll-up that significantly interacts with the opposite side of the mixing-layer. Two roll-ups are shown in the oval of frame 7.

There are two mechanisms at play in the formation and development of the coherent spanwise structures. First, there is a strong streamwise pressure gradient in front of each tab. This pressure gradient leads to the development and roll-up of spanwise vortices [21]. Second, there is a strong interaction among spanwise and streamwise vortices. Apparently, a combination of these two is causing a regular roll-up of large structures (spanwise vorticity) on the tab side of the jet, and when there are two tabs, these roll-ups occur in alternating sides of the mixing-layer. These spanwise roll-ups regularly interact with the opposite side of the mixing-layer in an asymmetric pattern

(a roll-up on one side of the mixing-layer generally corresponds to the region between adjacent roll-ups on the opposite side).

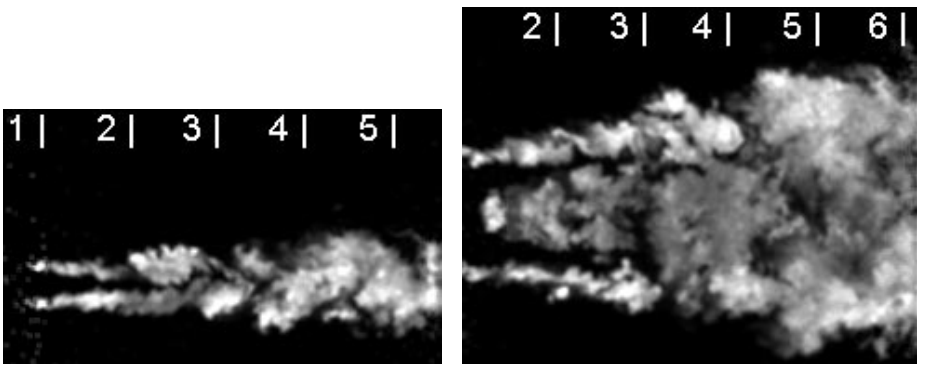

(a) (b)

Figure 10. Two instantaneous, streamwise images from a dual-tab jet showing the dynamics between 1 and 6 x/D. The illuminating and tab planes coincide in (a) and are normal in (b).

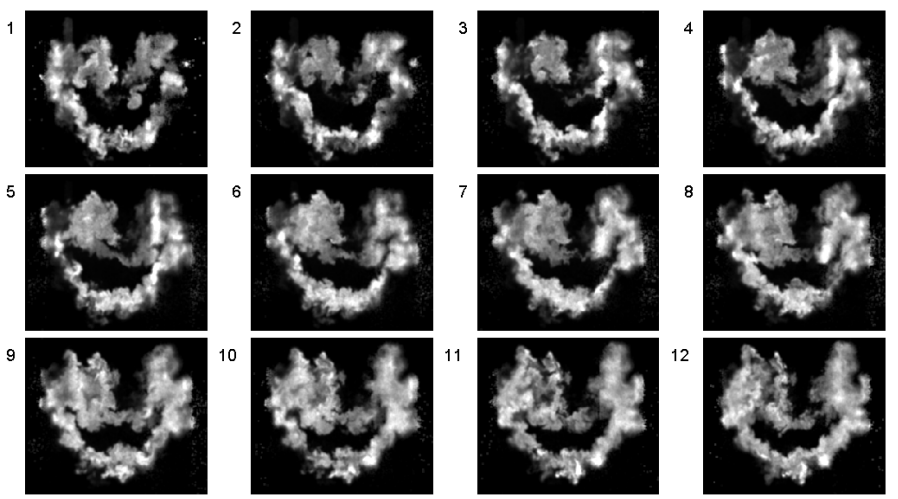

Figure 11. Example of a cross-stream image set from the single-tab jet showing a large, streamwise vortex in the upper left corner of the images.

Figure 11 shows a sequence of cross-stream plane images taken at 3 x/D. Past experience has shown that the overall effects of tab-generated streamwise vortices, schematically shown in Figure 2, are always obvious, but they are located outside of the deformed shear layer and thus very difficult to visualize [21]. However, the images in Figure 11 have captured the left corner vortex of the pair, which is rolling clockwise, as would be expected. The right corner vortex is not as large, or only a part of it has

been captured since there is no observed roll-up. The mixing-layer between the two vortices varies in thickness over the course of the images, but it is significantly below the two structures that dominate the top of the mixing-layer; this was quite typical for the cross-stream images. The cross-section of a dual-tab jet is the subject of the temporally resolved image set of Figure 12. As the spanwise roll-ups pass through the cross-stream image plane (at 3 x/D), they can be recognized as areas of mixed fluid that appear above and below the jet centerline. In the first frame of the image set, the top side of the central area (the 'circle' within the 'bowtie') has much more mixed fluid than the bottom side. By the fourth image, the bottom side has no mixed fluid while the top is quite large. Finally, in the eighth image, the area of mixed fluid has reversed with the bottom section, which is now much larger than the top. This matches quite well with the observed alternating spanwise roll-ups observed in Figure 9. Although an example was not presented in this work, spanwise activity was also observed in the single-tab images.

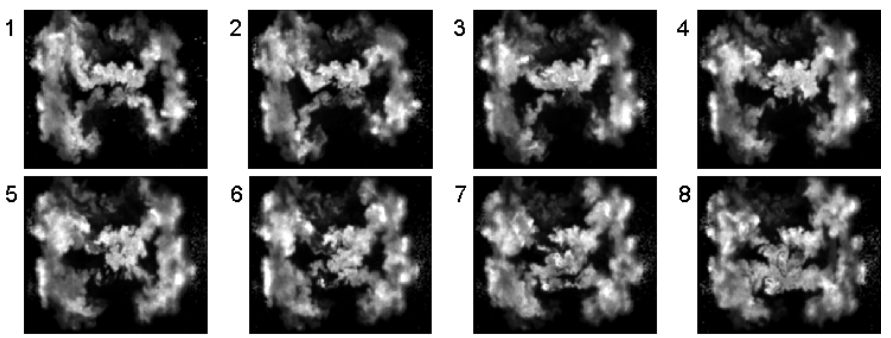

Figure 12. Example of a cross-stream image set from a dual-tab jet that shows significant cross-stream movement.

3.3. Acoustic power spectra

Power spectra of the far-field acoustic signal at microphone angles (θ) of 30˚, 60˚ and 90˚ were used to assess the effects of tabs on the jet's radiated sound field (Figure 13). To determine the azimuthal variation in the acoustic field, three azimuthal angles (ϕ) between the tab and the microphone for the single-tab jet (ϕ of 0˚, 90˚ and 180˚), and two azimuthal angles for the dual-tab jet (ϕ of 0˚ and 90˚) were studied in addition to a single azimuthal position for the baseline jet. These six measurements were made for each of the microphone angles (30˚, 60˚ and 90˚). The locations and conditions under study as well as their file nomenclature are summarized in the schematic of Figure 13 and Table 1. All of the spectra presented here were calculated from 10 seconds of data taken in blocks of 8192 points at a sampling rate of 200 kHz. The locations of the microphones were corrected to a distance of 60 jet diameters (1.5 m). The three microphones were located 96.0, 51.0 and 49.5D from the nozzle exit for the 30˚, 60˚ and 90˚ angles, respectively, and the locations were corrected to 60D by subtracting 6 dB from the SPL at all frequencies for every doubling of distance. The corrections were

thus 4.1, -1.6 and -1.7 dB for the 30˚, 60˚ and 90˚ locations respectively. Corrections to account for atmospheric absorption of higher frequency sound due to humidity or for standard day conditions were not performed (the consequences of which are discussed in reference 28). The power spectra are plotted against Strouhal number, $St_D = \frac{fD}{U}$, where D is the jet diameter (0.0254 m) and U is the jet exit velocity (380 m/s). These spectra are given in Figures 14 through 16 for the θ = 30˚, 60˚ and 90˚ positions, respectively.

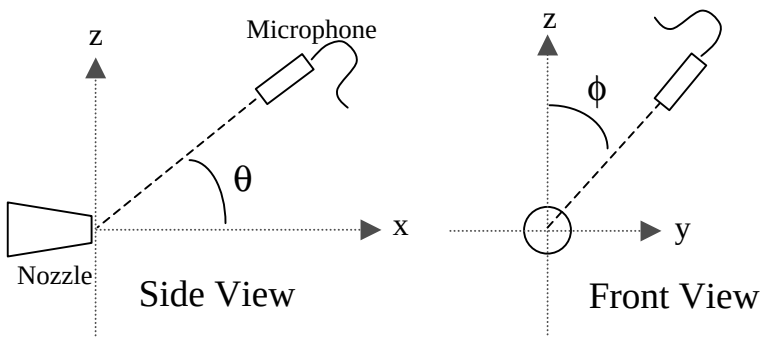

Figure 13. Schematic showing the reference system used in Figures 14 through 20. The tab(s) are located at [0.0 x/D, 0.0 y/D, 0.5 z/D] for the single-tab case and at [0.0 x/D, 0.0 y/D, ±0.5 z/D] for the dual-tab case.

Table 1. Nomenclature for the various downstream microphone locations and tab configurations.

Tab Configuration (microphone was located above nozzle)	Microphone location (Relative to Downstream Jet Centerline)		
	θ = 30˚	θ = 60˚	θ = 90˚
Baseline, no-tab, ring array data	ba_000_30	ba_000_60	ba_000_90
One, ϕ=0˚ offset from microphone	1t_000_30	1t_000_60	1t_000_90
One, ϕ=90˚ offset from microphone	1t_090_30	1t_090_60	1t_090_90
One, ϕ=180˚ offset from microphone	1t_180_30	1t_180_60	1t_180_90
Two, ϕ=0˚ offset with microphone	2t_000_30	2t_000_60	2t_000_90
Two, ϕ=90˚ offset from microphone	2t_090_30	2t_090_60	2t_090_90

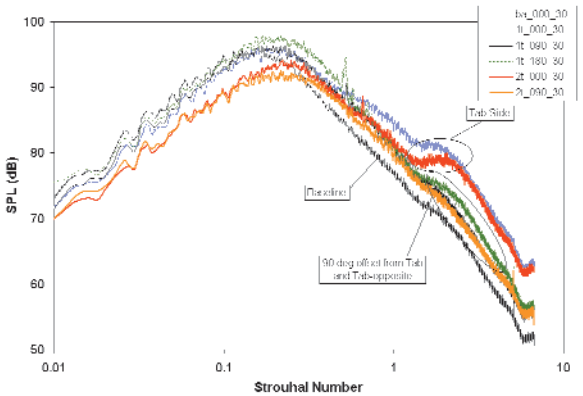

Figure 14. Comparison of the power spectra for the baseline, single-tab and dual-tab cases for the θ = 30˚ microphone location.

The addition of a single delta tab appears to increase the radiated sound in the θ = 30˚ direction for St_D above 0.1 without a substantial change at lower frequencies (Figure 14). This is true regardless of the relative azimuthal microphone location. When an additional delta tab is added to the nozzle lip (they are separated by 180˚ at the nozzle exit), SPL values below St_D of 0.25 are substantially reduced in both measured directions, while higher frequency noise is increased. The largest increase in the peak sound pressure over the baseline jet occurs with the addition of a single-tab at an azimuthal direction opposite the tab (ϕ=180˚, case 1t_180_30), and this increase is observed for St_D between 0.1 and 0.6. This direction possesses a narrow peak at St_D of 0.52, the origin of which is unclear. These spectra would need to be scaled to engine size and weighted for human annoyance to determine any actual noise reduction [8].

The aforementioned, high frequency increase in sound energy has a strong azimuthal dependence. Between St_D of 1 and 7, the tab-side of the jet (ϕ=0˚, cases 1t_000_30 and 2t_000_30) is much louder than the other azimuthal positions of the tabbed jets as well as the baseline case. The difference in the azimuthal directions is most dramatic in the region shown in the circle marked 'tab-side.' This peak marks a stark difference between the two azimuthal directions of a dual-tab jet (compare 2t_000_30 versus 2t_090_30). Below St_D of 1, the two azimuthal directions of the dual-tab jet deviate by less than 2 dB; however, above this value, the two directions deviate by as much as 7 dB. On a non-tab azimuthal direction (ϕ≠0˚, regardless of whether one or two tabs were on the jet: 1t_090_30, 1t_180_30 or 2t_090_30), there is a fairly uniform decrease in sound intensity with increasing frequency for St_D above 1, but on the tab side of the jet (ϕ=0˚, cases 1t_000_30 and 2t_000_30), there is the marked peak which is followed by a uniform decrease (for St_D above 2.5).

The power spectra taken at θ = 60˚ are shown in Figure 15. For St_D below 0.05, the addition of a single-tab does not change the radiated sound energy; however, for St_D above 0.05, there is a large increase in sound energy over the baseline case. The

maximum difference occurs for St_D between 1 and 2.5. The addition of two tabs decreases the sound energy for St_D below 0.15 and there is an increase above this value. Again, the maximum increase over the baseline case occurs for St_D between 1 and 3. Thus, one can see that the transitions from noise reduction to augmentation is different for the $\theta = 30^\circ$ and 60° spectra with a shift from St_D of 0.1 to 0.05 for the single-tab and from St_D of 0.25 to 0.15 for the dual-tab case. A consequence of the addition of the tabs to the jet is a broad but relatively well-defined acoustic peak at frequencies between St_D of 1 and 3. For a given tabbed jet, this peak reaches a maximum amplitude at an azimuthal position aligned with the tab ($\phi=0^\circ$, 1t_000_60 or 2t_000_60), i.e. the tab side is louder over the range of St_D between 1 and 3 than other azimuthal positions ($\phi\neq0^\circ$, 1t_090_60, 1t_180_60 or 2t_090_60). For St_D between 0.1 and 0.8, the tab-opposite side of the single-tab jet ($\phi=180^\circ$, 1t_180_60) is the loudest case; there was a similar range of frequencies at the 30° microphone direction where the single-tab jet ($\phi=180^\circ$, 1t_180_30) was loudest.

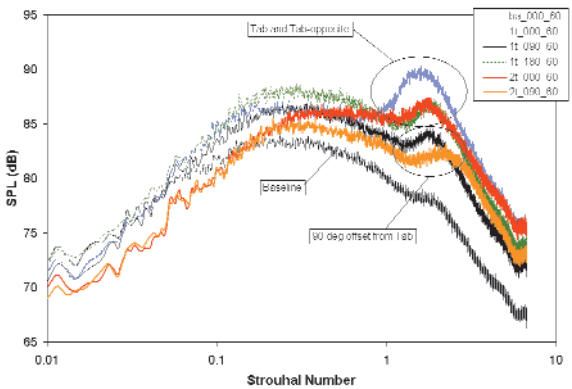

Figure 15. Comparison of the power spectra for the baseline, single-tab, and dual-tab cases for the $\theta = 60^\circ$ microphone location.

Not surprisingly, the $\theta = 90^\circ$ power spectra (Figure 16) bare many of the trends observed in the $\theta = 60^\circ$ case. At this microphone position, adding tabs (one or two) causes an increase in the acoustic field (relative to the baseline jet) at all frequencies and at all of the measured azimuthal directions with one exception. The dual-tab jet was quieter than the baseline jet for St_D below 0.1. The largest increase over the baseline jet occurs for St_D between 0.7 and 2. As observed at the other microphone locations ($\theta = 30^\circ$ and 60°), for St_D between 0.7 and 2 the tabbed side of the single ($\phi=0^\circ$, 1t_000_90) and dual-tab jets ($\phi=0^\circ$, 2t_000_90) have a higher sound intensity than the other azimuthal positions. One of the previously observed trends is not continued. At the other two microphone locations, the tab opposite single-tab case ($\phi=180^\circ$, 1t_180_90) has the highest SPL values over the range of St_D between 0.1 and 0.8; however, at the $\theta = 90^\circ$ microphone location, all of the spectra from the various tab geometries and azimuthal locations are nearly equal for St_D between 0.1 and 0.8.

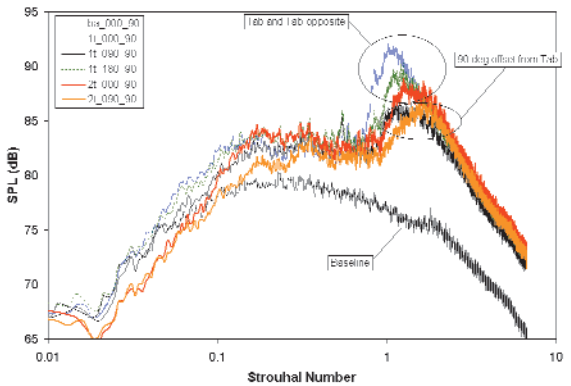

Figure 16. Comparison of the power spectra for the baseline, single-tab, and dual-tab cases for the θ = 90˚ microphone location.

3.4. Average acoustic waveform

Another means of determining the delta tab effect on sound emission is to compare an ensemble average waveform for the large amplitude sound pressure peaks. The waveform is created by phase-aligning acoustic peaks that have magnitude above a certain threshold (1.5σ for this study) and then ensemble averaging. This is performed in the time domain whereas acoustic spectra are an analysis in the frequency domain. The average waveform of the acoustic waves reaching the far-field reveals information that is not obvious from an acoustic spectrum. This was originally performed for the baseline Mach 1.3 jet at a microphone location of 30˚ in reference 3. That waveform had a strong resemblance to the acoustic field generated by the interaction (leapfrogging) of two ring vortices where the peak sound emission coincides with the two vortices passing through one another [29-31]. It is not known how the current results and the leapfrogging results are related, but the similarities are quite intriguing. Furthermore, the waveform was quite similar to a Mexican hat wavelet. Here, the effects of adding one or two delta tabs are examined on the positive waveform for the three microphone locations examined in the spectra of the last section (θ=30˚, 60˚ and 90˚). The average waveforms were created by first normalizing the acoustic data by their respective standard deviations, gathering 1 ms of data before and after all of the acoustic peaks that exceeded 1.5σ and then ensemble averaging these data. The data have been plotted against time that is non-dimensionalized by the convective velocity (U_c = 270 m/s) and the jet diameter. The convective velocity is used instead of the exit velocity to better relate the acoustic waveform to the time scale of the large-scale turbulence structures.

The average waveforms that were measured for the baseline jet at the three microphone locations (θ=30˚, 60˚ and 90˚) are compared in Figure 17. The most notable observation from these data is the stark difference in the waveform shapes for the three directions. The 30˚ location has a wave shape with distinct side lobes whereas

a single narrow peak without any side lobes dominates the 60˚ and 90˚ locations. The 30˚ waveform has a 3.2 time scale (0.3 ms) separation between its two negative side lobes and it is 0.6 time scales (0.06 ms) wide at amplitude of 1.0σ. However, the other two microphone locations do not have large side lobes and are less than 0.1 time scales (0.01 ms) wide at 1.0σ. The differences in the acoustic waveform widths can be directly correlated to the previously given acoustic spectra. The width of the 30˚ waveform would have a frequency of 0.3 ms^{-1}, which is 3 kHz or St_D of 0.2. This is close to the broadband peak of the 30˚ spectrum (around St_D = 0.15). The spectra for the 60˚ and 90˚ locations do not have any such peak as they are evenly distributed over a broad range of frequencies. This corresponds well to spectra that were created from the 60˚ and 90˚ waveforms (not shown here). This should not be surprising since a single peak in the time domain corresponds to a flat spectrum in the frequency domain. The time scales of the waveforms correlate well with the structure scales that are known to dominate the production of acoustic radiation in the two extreme directions (30˚ and 90˚). The larger scales, which have acoustic radiation that dominates at the 30˚ location, have a larger time scale than the smaller scales that radiate in the 90˚ direction. This observation matches the differences in acoustic waveform widths where the 30˚ waveform spans a much larger time than the 90˚ waveform. The 60˚ waveform has a shape that is quite similar to the 90˚ waveform, which is an indication that the generation of noise at this location is due to smaller scales as well.

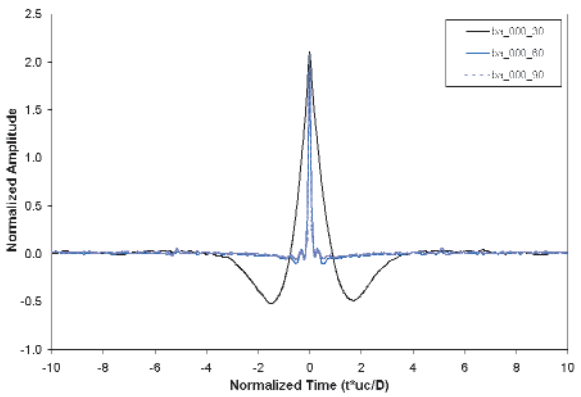

Figure 17. Comparison of the average acoustic waveforms for the three different microphone locations (θ = 30, 60 and 90˚) for the baseline, Mach 1.3 jet.

The acoustic waveforms for the single- and dual-tab jets are plotted against the baseline jet waveform for the 30˚, 60˚ and 90˚ locations in Figures 18 through 20, respectively. Interestingly, all of the waveforms have a central peak that reaches a maximum slightly above two. Apparently, the standard deviation is the correct normalization scale, as it non-dimensionalizes all of the cases to the same magnitude. The time scales for the 30˚, 60˚ and 90˚ locations were varied to show details of the central portion of the waveforms.

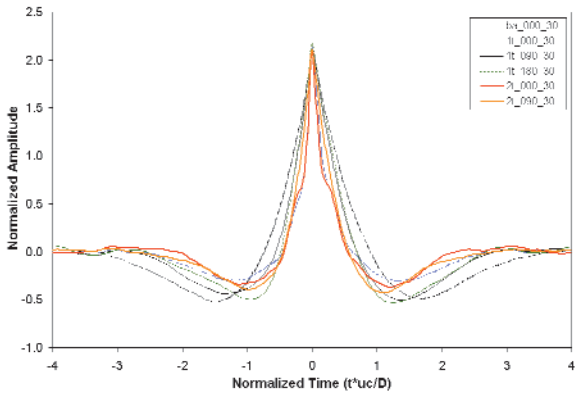

Figure 18. Comparison of the average acoustic waveforms for the θ = 30˚ location.

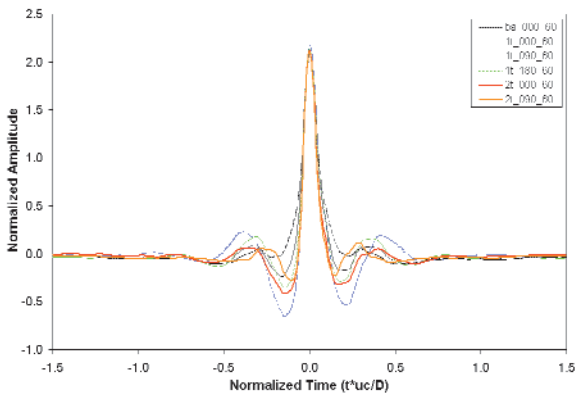

Figure 19. Comparison of the average acoustic waveforms for the θ = 60˚ location.

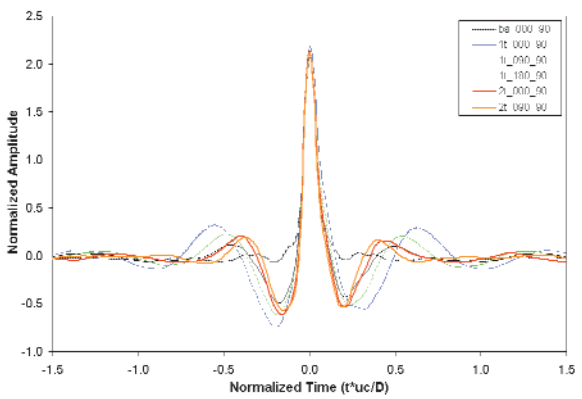

Figure 20. Comparison of the average acoustic waveforms for the θ = 90˚ location.

From Figure 18, one can see that the waveform for the microphone side, single-tab (1t_000_30) case has a narrower central peak and lower amplitude side lobes than the baseline case (ba_000_30). The 90˚ and 180˚, single-tab cases (1t_090_30 and 1t_180_30) are wider than the 0˚ case (1t_000_30), but are narrower than the baseline case (ba_000_30). Both the 0˚ and 90˚ dual-tab waveforms are narrower than the baseline waveform. The decrease in side lobe spacing correlates directly to the peak frequency shift of Figure 14. The separation between the side lobes for the baseline waveform (ba_000_30) is about 3 time scales (300 μsec); if this is the period of the waveform, then the corresponding frequency would be about St_D = 0.2 (3 kHz). The dual-tab waveforms (2t_000_30 and 2t_090_30) have a separation of about 2 time scales (200 μsec) or a frequency of about St_D = 0.3 (5 kHz). These correspond to the peak frequencies of Figure 14. A particularly interesting feature of the single and dual-delta tab configurations (ϕ=0˚, 1t_000_30 and 2t_000_30) is a sudden narrowing of the waveform at a normalized time of about ±0.2, which corresponds to a separation of 40 μsec and a frequency of St_D = 2 (25 kHz); thus, this narrowing of the waveform is the time domain representation of the differences between the tab-side spectra for St_D ~ 2.

The two acoustic waveforms (Figures 19 and 20) that were created from acoustic data taken at microphone locations of θ = 60˚ and 90˚ are similar in many aspects. Primarily, they are much narrower than those from the 30˚ microphone location, which is why they are plotted on a shorter scale (3 convective time scales versus 8). They also have one other common feature. Without tabs, the waveform for these locations does not have side lobes and their spectra are relatively flat (see Figures 15 and 16). However, with the addition of tabs, the waveforms have multiple side lobes that have a period that matches the broad spectral peaks over a range of St_D between 0.7 and 2. At the 30˚ microphone location, there was only one side lobe on either side of the main peak regardless of the configuration. The largest magnitude side lobes are on the tab side of the jet (ϕ=0˚, 1t_000_60, 1t_000_90, 2t_000_60 and 2t_000_90) and this matches the increase in the broad spectral peaks at this azimuthal location. These multiple side lobes are likely an indication of an increased level of coherence of the structures, dynamics of which are generating acoustic radiation at these angles. These results corroborate the visualization results shown in Figures 8 to 10, which show increased structure coherence for the tabbed jets.

There is a subtle difference between the tabbed waveforms for the θ = 60˚ and 90˚ microphone locations that was also observed in the spectra. The tabbed waveform side lobes for the θ = 60˚ location (ϕ=0˚, i.e. 1t_000_60) have a closer spacing than the θ = 90˚ location (i.e., 1t_000_90). This decreased period corresponds to an increase in frequency content, which was observed in their spectra. Apparently, the noise that is being generated decreases in frequency as one moves to a location that is closer to the jet exit. This is a trend that is opposite to that observed in jets that do not have streamwise vortex generating tabs and most likely is due to differences in the nature of the turbulence structure dynamics that are responsible for generating the peaks in the acoustic far field.

In summary, trends observed in the acoustic waveforms match those of the

acoustic power spectra. Both results showed that the addition of tabs caused an increase in high frequency noise (decrease in waveform side lobe widths) at the microphone location of $\theta = 30^\circ$. When the 30° microphone was aligned with the tab ($\phi=0^\circ$), the acoustic waveforms had an indentation that matches an increase in the high frequency acoustic spectra. Regardless of the microphone location or number of tabs used, acoustic spectra showed the tab side of the jet ($\phi=0^\circ$) increased high frequency acoustic radiation over other azimuthal directions ($\phi\neq0^\circ$). Similarly, the acoustic waveforms showed a narrowing of the waveforms for the tab side of the jet at $\theta = 30^\circ$ (Figure 18) and increased side lobe magnitude for the waveforms that were aligned with the tab at $\theta = 60^\circ$ and 90° (Figures 19 and 20).

3.5. Noise source distribution

Using the three-dimensional microphone array that was described in the experimental arrangement section, the origin for every peak with magnitude exceeding 1.5σ was determined for the baseline and tabbed jets. This technique finds the apparent source of individual sound 'waves' that have a peak amplitude above the set threshold. The streamwise (jet centerline), one-dimensional, and the cross-stream (plane normal to the jet centerline), two-dimensional, probability density distributions are shown in Figures 21 to 24 for each of the cases. For the single-tab case, the tab was located at the upper lip of the nozzle (0.0 x/D, 0.0 y/D, 0.5 z/D) and in the dual-tab case, the tabs were located on the nozzle exit at 0.0 y/D and ± 0.5 z/D. The amount of data analyzed for each of the three cases differed: 4.3 sec acquired for the baseline jet, 6.4 sec for the single-tab jet, and 6.5 sec for the dual-tab jet. This yielded 10,255, 19,526 and 20,573 acoustic peaks that exceeded 1.5σ, respectively, for the baseline, single and dual-tab jets (as determined by the top, front microphone of the array). The apparent noise origin for each of these peaks was determined with the 3-D microphone array.

It should be noted that this data set is different from that presented in reference 32 in two ways. First, that data set has been augmented by additional data that was subsequently acquired. Second, the acoustic data was low pass filtered at 10 kHz (St_D = 0.67), which was the highest frequency that could be accurately located with the 3-D microphone array [27]. The mean values for the x-direction given in reference 32 were 8.2, 3.3 and 2.9 for the baseline, single- and dual-tab jets, respectively (the values for the current work will be given shortly). The differences between the values here and those of reference 32 are due to the frequency filtering. The frequency filtering did not affect the measured y- and z-directions of the mean noise source locations.

The apparent noise source distributions in the streamwise direction for the Mach 1.3 jet with and without tabs are presented in the probability density plot of Figure 21. The bins are 1 x/D wide. The addition of tabs significantly shifts the noise generation regions of the jet. Comparing the mean values for the three distributions, which are 9.0, 3.8 and 4.5 x/D, respectively, for the baseline, single and dual-tab cases can quantify this. Without any tabs, eighty percent of the sound sources were located between 6 and 12 x/D. However, with a single-tab, 84% of the sources were

located between 1 and 6 x/D and with two tabs, 82% were located between 2 and 7 x/D. These results are qualitatively in agreement with the measurements of reference 10. They found the sound origins moved significantly upstream from a range of 4 to 8 x/D for a baseline jet to between 2 and 3 x/D for a jet with two rectangular, pointed tabs (the tabs were mounted normal to the jet centerline). With the noise source information and the streamwise flow images, some details of the mechanisms responsible for noise generation can be determined. The baseline jet has a mean noise source location of 9.0 x/D, which is in close proximity to where the top and bottom portions of the mixing-layers begin to interact in the average flow image (Figure 4b). Note that this location is not the end of the potential core, which was measured at an approximate location of 5.5 x/D [2]. The single-tab jet has a mean noise source location of 3.8 x/D, and this corresponds to where the two sides of the mixing-layer meet (Figure 5). However, the dual-tab jet has a mean noise source location of 4.5 x/D, which does not coincide with the end of the unmixed core of the jet (around 3 x/D, see Figure 6b). A further examination of the jet's noise distribution (specifically in the cross-stream direction) will clarify this discrepancy.

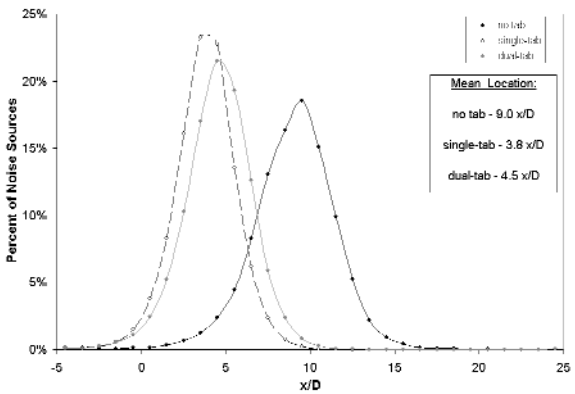

Figure 21. Comparison of the downstream noise source location for the baseline, single-tab, and dual-tab Mach 1.3 jets.

The y and z-components of the noise sources for the three cases are given in the 2-D probability density contour plots of Figures 22 through 24. Each of the plots covers the same area and the contour colors show the percent of apparent sound origins that came from each 0.05D by 0.05D bin. Also shown in the three plots are the relative positions of the nozzle lip line and tabs. The contour for the baseline jet in Figure 22 is circular with a slight offset from the origin. The mean values for this distribution are 0.1 y/D and 0.0 z/D. The small shift in the y-direction was consistent with all three configurations (the mean location varied between 0.1 and 0.2 y/D) and is likely due to the jet centerline being slightly skewed from a line normal to the microphone plane of the 3-D array [see reference 27 for 3-D array details]. Considering that the microphone array diameter was 52.0D, centering it to within 0.2D is quite good.

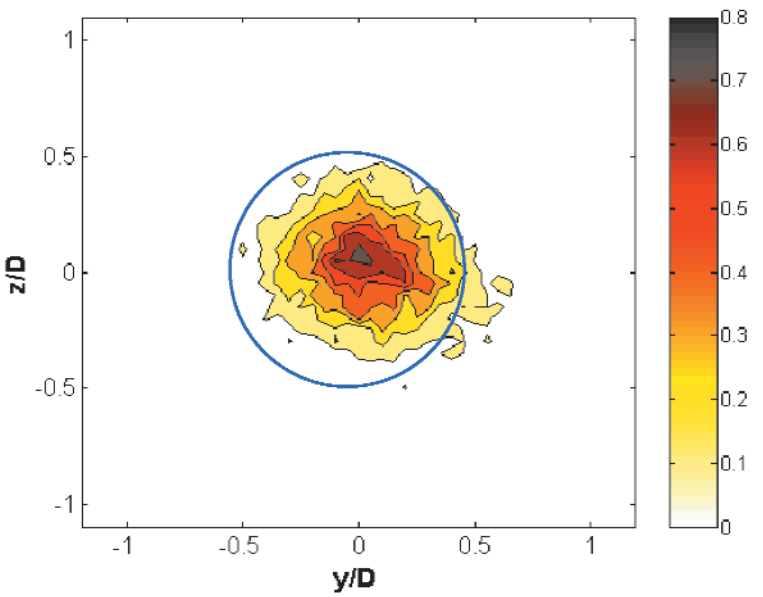

Figure 22. 2-D probability density distribution of apparent noise sources in the cross-stream plane for the baseline jet.

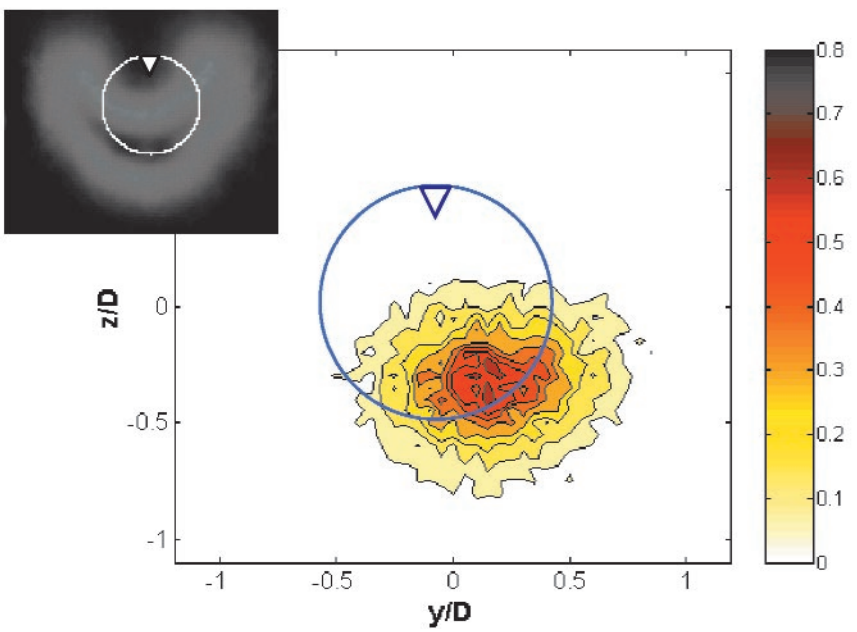

Figure 23. 2-D probability density distribution of apparent noise sources in the cross-stream plane for the single-tab jet. Image (b) of Figure 7 is included for comparison.

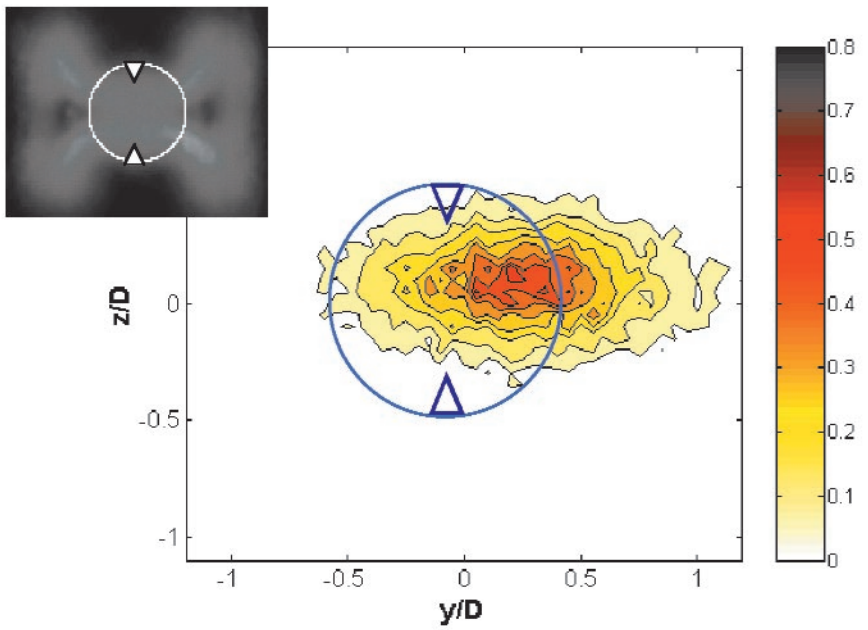

Figure 24. 2-D probability density distribution of apparent noise sources in the cross-stream plane for the dual-tab jet. Image (c) of Figure 7 is included for comparison.

The addition of a single-tab to the jet causes a dramatic shift in the y and z noise source components as shown in Figure 23. The apparent sound origins for the single-tab case have shifted relative to the circular distribution of the baseline jet as they are now centered below the jet centerline (mean locations of 0.2 y/D and -0.3 z/D). The addition of the delta tab has caused the noise origins to move away from the tab. This can be compared to the average cross-stream flow image (shown in upper left corner of figure) that was taken at a position of 3 x/D, which is close to the mean downstream noise source location. The majority of the noise sources correspond to the interaction region between the unaffected bottom mixing-layer and the deflected top mixing-layer. The deflection is due to the tab generated streamwise vortices. Of note, the largest concentration of noise sources is on and around the plane visualized in Figures 5 and 8. With all three components of the noise source location, it becomes clear that the region of noise generation corresponds to where the two sides of the mixing-layer are coming together. The mean streamwise noise source location matched this location in the average streamwise image, and the mean cross-stream noise source location coincides with this region in the average cross-stream image. Another key observation is that there was a negligible concentration of noise sources in the area where the streamwise vortices are observed, which are the upper right and left hand corners of the crescent shaped mixing-layer. One has to remember when analyzing these results that the

acoustic data was low pass filtered at 10 kHz prior to noise source analysis; hence, the noise sources are only for acoustic waves with frequency content less than 10 kHz. Apparently, either the streamwise vortices are not producing acoustic waves or the acoustic radiation has frequency content greater than 10 kHz. The noise source locations were also computed using the bottom front microphone data to identify the large amplitude events (instead of the top, front microphone) and the resulting distribution of noise sources was nearly identical to the single-tab data given in Figures 21 and 23.

When two tabs are placed on the jet exit, the cross-stream noise source distribution gets elongated along the y-axis as shown in Figure 24. The mean locations for the noise sources in these two directions are 0.2 y/D and 0.1 z/D. The elongation matches the central region of the average flow image (shown in upper left corner of figure) where spanwise roll-ups were growing and interacting on alternating sides of the mixing-layer (see Figures 9, 10 and 12). Again, the region where the counter-rotating streamwise vortices are present corresponds to a region lacking sound sources. The dual-tab jet has the largest concentration of noise sources in the region between the two tabs and this oval-shaped region falls on a plane that is normal to the plane formed by the two tabs. The average cross-stream image shows the majority of noise generation coincides with the region of the jet that is between the two unmixed cores of the bifurcated jet (the two cores are the black regions within the white 'bow-tie'). The noise generating region is best observed in the average image of Figure 6b and the instantaneous image of Figure 10b where the largest concentration of noise sources were in the central region of the jet over a downstream range between 2 and 7 x/D. Upstream of 3 x/D, the dual-tab jet is dominated by alternating large structure roll-ups. Downstream of 3 x/D, the jet is dominated by large structures that span the height (in the tab plane) and extend over the central portion of the jet, which is also the region of noise generation. Based on what is occurring within the region of sound generation, one would expect the dynamic interaction of these large, three-dimensional rolling structures to be responsible for the generation of sound. Such large structure dynamics (large structure interaction) was observed as a mechanism of sound generation within the baseline, Mach 1.3 jet [3].

4. SUMMARY AND CONCLUSIONS

The addition of delta tabs clearly introduced strong streamwise vortices to the mixing-layer of the jet, as it has been well known. This was deduced from the average cross-stream images of Figure 7. The addition of tabs also led to a more regular formation and roll-up of large-scale spanwise structures that form on the tab side of the mixing-layer. An example of such a roll-up was given in Figure 8. When two tabs were added to the jet, the structure roll-ups occurred on both sides of the mixing-layer in a staggered order as shown in the flow images of Figures 9, 10 and 12. The delta tabs also caused a shortening of the jet's unmixed core (compare Figures 4-6).

The delta tabs modified the azimuthal character of the jet's acoustic radiation at all measured microphone locations (θ=30˚, 60˚ and 90˚; see Figures 14 through 16). Regardless of the microphone location, the addition of one or two tabs to the jet caused an increase in high frequency acoustic levels on the tab side (ϕ=0˚) of the jet

relative to the other sides (ϕ=90˚ or 180˚) or the baseline case. The increase was observed for St_D between 0.7 and 2 depending on the microphone location. At microphone locations of 30˚ and 60˚, the side opposite of the tab in a single-tab configuration increased low frequency noise as compared to the other azimuthal angles or the baseline jet. These observations were also noticed in the average acoustic waveforms, which are the time domain representation of the radiated noise. Without the tab, the acoustic radiation was azimuthally uniform, but with the addition of either one or two delta tabs, the acoustic radiation became highly directional. The acoustic waveforms for the baseline jet at 30˚ and 90˚ had a distinct difference in their time scales, and this difference corresponds well with the turbulence structure scales that are thought to dominate acoustic radiation in these two directions (Figure 17). The acoustic waveforms of the tabbed jets were significantly different from the baseline case, especially at 60˚ and 90˚ (Figures 19 and 20) and had distinct properties that were dependent on the azimuthal location.

The distribution of apparent sound origins was also dramatically changed by the addition of delta tabs. Without any tabs, the sound origin distribution was centered along the jet centerline (Figure 22) with a mean downstream location of 9.0 x/D. When a single-tab was added at the jet exit, the mean value of the downstream distribution shifted upstream to 3.8 x/D (Figure 21) while the cross-stream distribution was deflected away from the tab (Figure 23). A dual-tab jet had a mean downstream location of 4.5 x/D (Figure 21), and an oval distribution in the cross-stream plane (Figure 24).

The observed changes in the acoustic radiation of the jet could be explained if dynamics of the tab-generated, counter-rotating, vortex pairs were radiating sound at high frequencies. The various data presented in this work support such a hypothesis. There was a dramatic increase in acoustic radiation for St_D between 0.7 and 2 on the tab side of the jet as compared to the other measured azimuthal locations (see Figures 14 through 16). At a 30˚ microphone position, where the 3-D microphone array was located, the increase was largest around St_D of 2, which corresponds to a frequency of 30 kHz (Figure 14). Acoustic data was low pass filtered at 10 kHz prior to noise source location processing, thus the noise source location routine would not determine origins for any such sound waves. If dynamics of the counter-rotating streamwise vortices were generating acoustic radiation in excess of 10 kHz, then there would not be any noise sources (as determined by the 3-D array) in that region. This is exactly what was observed in Figures 23 and 24 where there was a lack of noise sources in the areas that were occupied by the counter-rotating streamwise vortex pairs. Therefore, it appears that the counter-rotating vortices were involved in the creation of acoustic radiation at frequencies above 10 kHz (St_D of 0.7). Since this radiation was being created on the tab-side of the jet, it would also be most prevalent on that side of the jet. The tabs also appeared to be altering the radiation of sound at frequencies that are typically associated with the larger scale turbulence structures ($St_D < 0.7$). Such analysis is best done at the 30˚ microphone position where the noise from larger scales dominates.

The 3-D microphone array, which was located at the 30˚ position, determined that

the vast majority of the single-tab jet noise sources had a downstream location between 1 and 6 x/D (see Figure 21). This region corresponds to the area where spanwise vortices were regularly rolling up in the top half of the mixing-layer and interacting with the bottom half of the mixing-layer (see Figure 8). This interaction region was on the opposite side of the jet from the counter-rotating streamwise vortices and was the region where the noise sources were observed in the cross-stream noise distribution of Figure 22. A link between structure roll-up, mixing-layer interaction and noise generation has been established [2-3]; hence, one would expect an area of structure roll-up with strong cross mixing-layer interaction to be responsible for the generation of significant sound. At the $\theta = 30^{\circ}$ microphone position, the most intense acoustic radiation was produced opposite the tab of a single-tab configuration at a St_D of 0.2 (3 kHz), which was slightly higher than the peak of the baseline jet (St_D of 0.15). If these roll-ups colliding with the mixing-layer were the cause of the sound production, then one would expect the maximum acoustic radiation to be on the same side of the jet as the interactions, which was the case.

A dual-tab jet had noise generation that appeared to be due to the complex dynamics that were occurring downstream the bifurcated potential cores of the jet. The maximum concentration of noise sources corresponds to a region between 2 and 7 x/D along a plane that was located between the two sets of streamwise vortices (see Figures 21 and 24). This region of the jet included the ends of the unmixed cores of the jet (~3 x/D, see Figure 6), had a great deal of three-dimensional motion (see Figure 10), and was located downstream of a region dominated by asymmetric structure roll-ups (see Figure 9). The tab side of the dual-tab jet ($\phi=0^{\circ}$) had a higher sound pressure at all frequencies than the non-tab side ($\phi=90^{\circ}$).

The tabs were causing large spanwise roll-ups to occur more regularly and robustly than was observed in a baseline jet. The regular formation of spanwise roll-ups and their interactions likely caused the shift in the peak of the frequency spectrum. They might also be the cause of the $St_D = 0.52$ peak in the acoustic spectrum for the single-tab jet (0° azimuthal separation) as well as the $St_D = 0.66$ peak in the acoustic spectrum for the dual-tab jet (0° azimuthal separation), but additional work would be needed to conclusively prove it.

In conclusion, it seems that the counter-rotating vortex pairs that were generated by the tabs were generating sound at high frequencies ($St_D \sim 2$, which was significantly higher than the peak baseline jet noise of $St_D \sim 0.15$ at a 30° microphone position) that preferentially radiated in the tab direction. The tabs also seem to regulate the formation of spanwise roll-ups, which had a strong influence on the peak jet noise ($St_D \sim 0.2$) at the 30° downstream position.

ACKNOWLEDGMENT

The Air Force Office of Scientific Research, with Dr. John Schmisseur as the Technical Monitor, sponsored this work. The authors are grateful to Brian Thurow for his assistance in taking the temporally resolved flow visualization images and fruitful discussions. The first author would like to thank the Ohio Space Grant Consortium for his Doctoral Fellowship.

REFERENCES

1. Lighthill, M.J. (1952) On Sound Generated Aerodynamically: I. General Theory. *Proc. Royal Soc. London*, Ser. A., Vol. 211, pp. 564-581, 1952.
2. Hileman, J. and Samimy, M. (2001) "Turbulence Structures and the Acoustic Far-Field of a Mach 1.3 Jet," *AIAA Journal*, Vol. 39, No. 9, 2001, pp. 1716-1727.
3. Hileman, J., Thurow, B. and Samimy, M. (2002) "Exploring Noise Sources Using Simultaneous Acoustic Measurements and Real-Time Flow Visualizations in Jets," *AIAA Journal*, Vol. 40, No. 12, 2002, pp. 2382-2392.
4. Tam, C.K.W. (1991) "Jet Noise Generated by Large-Scale Coherent Motion." *Aeroacoustics of Flight Vehicles: Theory and Practice. Vol. 1*, edited by H.H. Hubbard, 1991, pp. 311-390.
5. Morrison, G.L and McLaughlin, D.K. (1979) "Noise Generation by Instabilities in Low Reynolds Number Supersonic Jets," *Journal of Sound and Vibration*, Vol. 65, 1979, pp. 177-191.
6. Yu, J.C. and Dosanjh, D.S. (1972) "Noise Field of a Supersonic Mach 1.5 Cold Model Jet," *Journal of the Acoustical Society of America*, Vol. 51, No. 5, Pt. 1, 1972, pp. 1400-1410.
7. Schaffar, M. (1979) "Direct Measurements of the Correlation Between Axial in-jet Velocity Fluctuations and Far-field Noise near the Axis of a Cold Jet," *Journal of Sound and Vibration*, Vol. 64, No. 1, 1979, pp. 73-83.
8. Simonich, J.C., Narayanan, S., Barber, T.J. and Nishimura, M. (2001) "Aeroacoustic Characterization, Noise Reduction, and Dimensional Scaling Effects of High Subsonic Jets," *AIAA Journal*, Vol. 39, No. 11, 2001. pp. 2062-2069.
9. Ahuja, K.K., Massey, K.C. and D'Agostino, M.S. (1998) "A Simple Technique of Locating Noise Sources of a Jet Under Simulated Forward Motion," *AIAA Paper* 98-2359, 1998.
10. Fisher, M.J., Harper-Bourne, M. and Glegg, S.A.L. (1977) "Jet Engine Source Location: The Polar Correlation Technique," *Journal of Sound and Vibration*, Vol. 51, No. 1, 1977, pp. 23-54.
11. Kibens, V. (1980) "Discrete Noise Spectrum Generated by an Acoustically Excited Jet," *AIAA Journal*, Vol. 18, 1980, pp. 434-441.
12. Colonius, T., Lele, S. and Moin, P (1997) "Sound Generation in a Mixing-layer," *Journal of Fluid Mechanics*, Vol. 330, August 1997, pp. 375-409.
13. Mitchell, B., Lele, S. and Moin, P. (1998) "Direct Computation of the Sound Generated by Vortex Pairing in an Axisymmetric Jet," *Journal of Fluid Mechanics*, Vol. 383, October 1998, pp. 113-142.
14. Bridges, J. and Hussain, F. (1992) "Direct evaluation of aeroacoustic theory in a jet," *Journal of Fluid Mechanics*, Vol. 240, 1992, pp. 469-501.
15. Freund, J. (2001) "Noise sources in a low-Reynolds-number turbulent jet at Mach 0.9," *Journal of Fluid Mechanics*, 2001, vol. 438, pp. 277-305.

16. Sarohia, V. and Massier, P.F. (1977) "Experimental Results of Large-scale Structures in Jet Flows and Their Relation to Jet Noise Production," AIAA Paper 77-1350, 1977.
17. Thurow, B., Samimy, M. and Lempert, W. (2003) "Compressibility Effects on Turbulence Structures of Axisymmetric Mixing Layers," *Physics of Fluids*, Vol. 15, No. 6, 2003, pp. 1755-1765.
18. Ahuja, K.K and Brown, W.H. (1989) "Shear Flow Control by Mechanical Tabs," AIAA Paper No. 89-0994, 1989
19. Samimy, M., Zaman, K.B.M.Q. and Reeder, M. (1993) "Effect of Tabs on the Flow and Noise Field of an Axisymmetric Jet," *AIAA Journal*, Vol. 31, No. 4, 1993, pp. 609-619.
20. Bradbury, L.J.S. and Khadem, A.H. (1975) "The Distortion of a Jet by Tabs," *Journal of Fluid Mechanics*, Vol. 70, 1975, pp. 801-813.
21. Zaman, K.B.M.Q., Reeder, M.F. and Samimy, M. (1994) "Control of an Axisymmetric Jet Using Vortex Generators," *Physics of Fluids*, Vol. 6, No. 2, 1994, pp. 778-793.
22. Reeder, M.F. and Samimy, M. (1996) "The evolution of a jet with vortex-generating tabs: real-time visualization and quantitative measurements," *Journal of Fluid Mechanics*, Vol. 311, 1996, pp. 73-118.
23. Reeder, M.F., Samimy, M. and Elliott, G. (1996) "Investigation of the Effect of Tabs on Supersonic Jets Using Advanced Diagnostics," *Journal of Propulsion and Power*, Vol. 12, No. 4, 1996, pp. 742-751.
24. Clancy, P. (1997) *Development and Application of Three-Component Planar Doppler Velocimetry for High Speed Flows*. PhD thesis, The Ohio State University, Dept of Mechanical Engineering, 1997.
25. Tam, C.K.W. and Zaman, K.B.M. (2000) "Subsonic Jet Noise from Nonaxisymmetric and Tabbed Nozzles," *AIAA Journal*, Vol. 38, No. 4, 2000, pp. 592-599.
26. Kerechanin, C.W., Samimy, M. and Kim, J.-H. (2001) "Effects of Nozzle Trailing Edges on Acoustic Field of Supersonic Rectangular Jet," *AIAA Journal*, Vol. 39, No. 6, 2001, pp. 1065-1070.
27. Hileman, J., Thurow, B. and Samimy, M. (2002) "Development and Evaluation of a 3-D Microphone Array to Locate Individual Acoustic Sources in A High Speed Jet," to appear *Journal of Sound and Vibration* in 2003.
28. Viswanathan, K. (2002) "Analysis of the Two Similarity Components of Turbulent Mixing Noise," *AIAA Journal*, Vol. 40, No. 9, 2002, pp. 1735-1744.
29. Bridges, J. and Hussain, F. (1995) "Effects of Nozzle Body on Jet Noise," *Journal of Sound and Vibration*, Vol. 188, No. 3, 1995, pp. 407-418.
30. Tang, S.K. and Ko, N.W.M. (1993) "A Study on the Noise Generation Mechanism in a Circular Air Jet," *Journal of Fluids Engineering*, Vol. 115, No. 3, 1993, pp. 425-435.

31. Inoue, O. (2002) "Sound generation by the leapfrogging between two coaxial vortex rings," *Physics of Fluids*, Vol. 14, No. 9, 2002, pp. 3361-3364.
32. Hileman, J. and Samimy, M. (2002) "Effects of Vortex Generating Tabs on Noise Sources in an Ideally Expanded Mach 1.3 Jet," AIAA Paper 2002-2482, 2002.